Experimental Neurology 374 (2024) 114704

Contents lists available at ScienceDirect

Experimental Neurology

journal homepage: www.elsevier.com/locate/yexnr

Research paper

Positive relation between dopamine neuron degeneration and metabolic connectivity disruption in the MPTP plus probenecid mouse model of Parkinson's disease

Margherita Tassan Mazzocco [a,b,1], Marcello Serra [c,1], Marco Maspero [b,d], Angela Coliva [b], Luca Presotto [b,e], Maria Antonietta Casu [f], Micaela Morelli [c,g], Rosa Maria Moresco [b,d,h,*], Sara Belloli [b,d,2], Annalisa Pinna [g,2]

[a] PhD Program in Neuroscience, Medicine and Surgery Department, University of Milano-Bicocca, Monza, Italy
[b] Nuclear Medicine Department, San Raffaele Scientific Institute (IRCCS), Milan, Italy
[c] Department of Biomedical Sciences, Section of Neuroscience, University of Cagliari, Cagliari, Italy
[d] National Research Council of Italy, Institute of Molecular Bioimaging and Physiology, UOS of Segrate, Italy
[e] Department of Physics "G. Occhialini", University of Milano - Bicocca, Milan, Italy
[f] National Research Council of Italy, Institute of Translational Pharmacology, UOS of Cagliari, Scientific and Technological Park of Sardinia POLARIS, Pula, Italy
[g] National Research Council of Italy, Neuroscience Institute, UOS of Cagliari, Italy
[h] School of Medicine and Surgery, University of Milano - Bicocca, Monza, Italy

ARTICLE INFO

Keywords:
Dopamine transporter
Tyrosine hydroxylase
Connectome
FDG
Biomarker
Striatum
Substantia nigra
Subchronic MPTP
Emission tomography

ABSTRACT

The clinical manifestation of Parkinson's disease (PD) appears when neurodegeneration is already advanced, compromising the efficacy of disease-modifying treatment approaches. Biomarkers to identify the early stages of PD are therefore of paramount importance for the advancement of the therapy of PD. In the present study, by using a mouse model of PD obtained by subchronic treatment with the neurotoxin 1-methyl-4-phenyl-1,2,3,6-tetrahydropyridine (MPTP) and the clearance inhibitor probenecid (MPTPp), we identified prodromal markers of PD by combining *in vivo* positron emission tomography (PET) imaging and *ex vivo* immunohistochemistry. Longitudinal PET imaging of the dopamine transporter (DAT) by [^{18}F]-*N*-(3-fluoropropyl)-2β-carboxymethoxy-3β-(4-iodophenyl) nortropane ([^{18}F]-FP-CIT), and brain glucose metabolism by 2-deoxy-2-[^{18}F]-fluoroglucose ([^{18}F]-FDG) were performed before MPTPp treatment and after 1, 3, and 10 MPTPp administrations, in order to assess relation between dopamine neuron integrity and brain connectivity. The results show that *in vivo* [^{18}F]-FP-CIT in the dorsal striatum was not modified after the first administration of MPTPp, tended to decrease after 3 administrations, and significantly decreased after 10 MPTPp administrations. Post-mortem immunohistochemical analyses of DAT and tyrosine hydroxylase (TH) in the striatum showed a positive correlation with [^{18}F]-FP-CIT, confirming the validity of repeated MPTPp-treated mice as a model that can reproduce the progressive pathological changes in the early phases of PD. Analysis of [^{18}F]-FDG uptake in several brain areas connected to the striatum showed that metabolic connectivity was progressively disrupted, starting from the first MPTPp administration, and that significant connections between cortical and subcortical regions were lost after 10 MPTPp administrations, suggesting an association between dopamine neuron degeneration and connectivity

Abbreviations: PD, Parkinson's disease; MPTP, 1-methyl-4-phenyl-1,2,3,6-tetrahydropyridine; MPTPp, MPTP + probenecid; VEH, vehicle; DAT, dopamine transporter; [^{18}F]-FP-CIT, [^{18}F]-N-(3-fluoropropyl)-2β-carboxymethoxy-3β-(4-iodophenyl) nortropane; [^{18}F]-FDG, 2-deoxy-2-[^{18}F]-fluoroglucose; PET, positron emission tomography; SPECT, single-photon emission computed tomography; MRI, magnetic resonance imaging; TH, tyrosine hydroxylase; LBD, Lewy body dementia; iRBD, idiopathic rapid eye movement sleep behaviour disorder; UPDRS, Unified Parkinson's Disease Rating Scale; ARRIVE, Animal Research: Reporting of *In Vivo* Experiments; PFA, paraformaldehyde; PB, phosphate buffer; PBS, phosphate buffer saline; DAB, diaminobenzidine; NGS, normal goat serum; SNc, substantia nigra pars compacta; DS, dorsal striatum; midB, midbrain; MO, somatomotor cortical areas; SS, somatosensory cortical areas; Thal, thalamus; *VS*, ventral striatum.

* Corresponding author at: Department of Medicine and Surgery, University Milan-Bicocca, Milan, Italy.
E-mail address: rosa.moresco@unimib.it (R.M. Moresco).

[1] Margherita Tassan Mazzocco and Marcello Serra contributed equally to this work.
[2] Sara Belloli and Annalisa Pinna contributed equally to this work.

https://doi.org/10.1016/j.expneurol.2024.114704
Received 11 October 2023; Received in revised form 15 January 2024; Accepted 25 January 2024
Available online 26 January 2024

disruption in this PD model. The results of this study provide a relevant model, where new drugs that can alleviate neurodegeneration in PD could be evaluated preclinically.

1. Introduction

Parkinson's disease (PD) is characterized by the progressive loss of nigrostriatal dopaminergic neurons and the accumulation of misfolded proteins, such as α-synuclein, in the form of Lewy bodies (Obeso et al., 2017). These events lead to a broad spectrum of clinical manifestations, including cardinal motor dysfunctions, as well as non-motor and cognitive impairments (Jankovic, 2008; Obeso et al., 2017).

The diagnosis of PD primarily relies on the clinical evaluation of the patient's symptoms. In the prodromal phases of PD, the symptoms are typically mild and encompass olfactory deficits, sleep disorders, and constipation. In the later phases, symptoms become more pronounced and debilitating, featuring bradykinesia, muscle rigidity, resting tremor, gait disorders, and postural instability (Chaudhuri and Schapira, 2009; Jankovic, 2008; Obeso et al., 2017). PD diagnosis also benefits from the utilization of diagnostic imaging techniques, such as magnetic resonance imaging (MRI), single-photon emission computed tomography (SPECT), and positron emission tomography (PET). These techniques enable the non-invasive detection of neuromorphological and biochemical alterations occurring in the brain of patients with PD (Bidesi et al., 2021).

Over the past few decades, a growing body of evidence has highlighted the heterogeneous nature of PD in terms of manifestation, disease onset, progression, and symptomatology. To mitigate the incidence of misdiagnosis and identify optimal therapeutic strategies, several biomarkers have been identified thus far and associated with either the idiopathic or the familial forms of PD, as well as the risk factors involved in PD development (Ascherio and Schwarzschild, 2016; Tolosa et al., 2021). In particular, a subset of these biomarkers, based on the use of PET/SPECT (regional brain metabolism and dopaminergic synaptic density) or MRI (water mobility and neuromelanin sensitive sequences), has been identified as established or emerging through the use of neuroimaging techniques (Mitchell et al., 2021).

The dopamine transporter (DAT) has been widely applied in research as well as in clinical practice to monitor the decline in dopaminergic function in patients with PD (Simuni et al., 2018; Stoessl, 2007). Interestingly, loss of putaminal DAT evaluated by SPECT has been correlated with both subtle motor impairments, such as reduced finger-tapping speed, and non-motor symptoms, such as hyposmia, in prediagnostic PD individuals, thus supporting its potential use as an early biomarker in PD (Noyce et al., 2018). Nevertheless, it is important to emphasize that striatal DAT neuroimaging manifested significant limitations when assessing the progression of the pathology in its advanced stages or attempting to predict the loss of dopaminergic neurons in the substantia nigra pars compacta (SNc) (Matuskey et al., 2020; Perlmutter and Norris, 2014). As indicated by post-mortem evaluations, this phenomenon is likely attributed to the nearly complete depletion of nigrostriatal dopaminergic terminals already apparent in patients exhibiting only mild or moderate clinical symptoms (Kordower et al., 2013). Given this, the combined use of alternative neuroimaging biomarkers, capable of overcoming such limitations, could be of paramount importance in clinical practice.

The uptake of 2-deoxy-2-[^{18}F]-fluoroglucose ([^{18}F]-FDG) is related to neuronal activity and synaptic integrity and has also demonstrated successful utilization as an imaging biomarker in the investigation of the preclinical stages of PD (Meles et al., 2021). Additionally, at follow-up, it exhibited remarkable accuracy in comparison with clinical evaluation in the context of differential diagnosis of PD with multiple system atrophy, progressive supranuclear palsy, and corticobasal degeneration (Eckert et al., 2005). In a recent neuroimaging study employing [^{11}C]-2β-carbomethoxy-3β-(4-fluorophenyl) tropane ([^{11}C]-CFT) for DAT and [^{18}F]-FDG as radiotracers, it was found that all patients with PD included in the study exhibited notable variations in radiotracer uptake within the basal ganglia (Li et al., 2020). Conversely, in several cortical regions, such as the frontal, parietal, temporal, and occipital cortices, the authors observed a modest reduction in radiotracer uptake, affecting only half of the patient's cohort with PD (Li et al., 2020). The evaluation of [^{18}F]-FDG regional uptake also allows the reconstruction of metabolic connectivity and the identification of disease-associated patterns for different neurodegenerative disorders, since regions with correlated [^{18}F]-FDG uptake values are functionally connected (Horwitz et al., 1984; Perovnik et al., 2023). Specifically, Boccalini and colleagues investigated metabolic connectivity in Lewy body dementia (LBD), PD, and idiopathic rapid eye movement sleep behaviour disorder (iRBD), as a potential marker characterizing the prodromal phase of different forms of parkinsonism (Boccalini et al., 2022; Postuma et al., 2019). The findings of this study revealed a distinctive pattern of connectivity reconfiguration in stable PD, primarily involving the motor and somatosensory networks. In contrast, iRBD exhibited a metabolic connectivity pattern that was more similar to that observed in individuals with LBD (Boccalini et al., 2022). These results, although based on a small cohort of patients, show the potential usefulness of metabolic connectivity in predicting disease evolution during the prodromal phases of the neurodegenerative process. Metabolic connectivity studies have allowed the identification of a PD-related pattern of metabolic alterations, characterized by hypermetabolism in a few areas, such as the thalamus, cerebellum, lentiform nucleus, and pons, and hypometabolism in the parieto-occipital and prefrontal cortices (Eidelberg et al., 1994; Matthews et al., 2018). Of note, these PD-related metabolic alterations exhibit a positive correlation with the motor symptoms part of the Unified Parkinson's Disease Rating Scale (UPDRS) and display some variations with age (Matthews et al., 2018). Interestingly, the expression of a PD-related pattern has been found to be elevated in iRBD patients compared with controls (Holtbernd et al., 2014). This is noteworthy, considering the estimation indicating that over 76% of patients with iRBD develop various forms of parkinsonism, such as PD, LBD, and multiple system atrophy, in an approximate time frame of 12 years (Iranzo et al., 2013; Postuma et al., 2019; Schenck et al., 2013), suggesting a potential application as a prodromal biomarker.

Starting from the relevance of biomarkers associated with the prodromal stages of PD, the present research focuses on characterizing the relationship between *in vivo* and *ex vivo* biomarkers and the progression of PD in a well-established animal model of PD, with the final goal to provide new tools for assessing the efficacy of new drugs in counteracting dopaminergic neurodegeneration. To this scope, we used the subchronic 1-methyl-4-phenyl-1,2,3,6-tetrahydropyridine (MPTP) mouse model in combination with the uricosuric agent probenecid (MPTPp) that, by delaying the clearance of the toxic metabolites of MPTP, allows a progressive and moderate loss of neurons in SNc, resembling the pathological condition observed in patients with PD (Bové and Perier, 2012; Francardo et al., 2017; Meredith and Rademacher, 2011; Schintu et al., 2009). This subchronic MPTPp model recapitulates the course of PD pathology in the early and presymptomatic phases of the disease (Baranyi et al., 2016; Serra et al., 2023), providing a useful tool to investigate the mechanisms underlying the progression of PD-associated neurodegeneration (Baranyi et al., 2016; Blandini and Armentero, 2012; Petroske et al., 2001; Schintu et al., 2009). Importantly, the neurotoxic events are long-lasting since they can still be detected up to 6 months after withdrawal from treatment (Petroske et al., 2001; Serra et al., 2023).

Based on these considerations, in the present study PET imaging studies (*in vivo* DAT and [^{18}F]-FDG, for dopamine neuron degeneration

and metabolic connectivity, respectively) were correlated to DAT and tyrosine hydroxylase (TH) *ex vivo* evaluation in the striatum and SNc of subchronic MPTPp-treated mice, in order to assess the correlation existing between these biomarkers and the progression of nigrostriatal neurodegeneration.

2. Materials and methods

2.1. Animals

Male C57BL/6J mice (age, 6 months; mean weight, 32 g) were purchased from ENVIGO (San Pietro al Natisone, Italy). Animals were housed in the San Raffaele Scientific Institute animal facility under constant temperature and humidity, with a 12-h light/dark cycle and access to food and water *ad libitum*. Experimental procedures involving the use of animals complied with the EU Directive 2010/63/EU for animal experiments and were approved by the Ethical Committees of the San Raffaele Research Institute (Milan, Italy) and the Italian Ministry of Health (licence no. 800/2020-PR). The study was carried out in compliance with the Animal Research: Reporting of *In Vivo* Experiments (ARRIVE) guidelines.

2.2. Drugs

1-methyl-4-phenyl-1,2,3,6-tetrahydropyridine (MPTP) and probenecid were purchased from DBA Italia S.r.l. (Segrate, Italy). MPTP was dissolved in 0.9% saline solution, while probenecid was dissolved in 5% sodium hydrogen carbonate ($NaHCO_3$).

2.3. Study design and experimental model

To generate the progressive MPTP plus probenecid (MPTPp) model of PD, C57BL/6J mice (n = 10) were injected intraperitoneally (i.p.) with of the clearance inhibitor probenecid (100 mg/kg), followed by the neurotoxin MPTP (25 mg/kg) after a 30-min interval, as previously described (Choi et al., 2018). MPTPp treatment was carried out twice a week, for a total of 5 consecutive weeks. Immediately after the first MPTPp administration, 4 mice died, hence the sample size became 6 mice.

Mice were monitored with PET-computed tomography (CT) imaging before treatment and after 1, 3, and 10 MPTPp administrations (Fig. 1A). In detail: before treatment, all mice (n = 10) underwent PET-CT with the DAT ligand [^{18}F]-*N*-(3-fluoropropyl)-2β-carboxymethoxy-3β-(4-iodophenyl)nortropane ([^{18}F]-FP-CIT) (week 1) and [^{18}F]-FDG (week 2); after 1 administration, they underwent PET-CT with [^{18}F]-FDG only (week 4; n = 6); after 3 administrations, they underwent [^{18}F]-FP-CIT (week 5; n = 6); and finally, after 10 administrations, they underwent PET-CT with both radiotracers (week 9–10; n = 6). Moreover, after 3 and 10 administrations (week 5 and 9), their motor behaviour was evaluated and compared with a group of mice treated in parallel with the same number of vehicle (VEH) administrations (n = 10) (Fig. 1A).

After the last PET acquisition, mice were sacrificed by transcardial perfusion and brains were collected for post-mortem immunohistochemical analysis (week 11).

Based on the [^{18}F]-FDG PET results, we decided to perform an additional experiment to investigate DAT binding at earlier time points, specifically one day after the first MPTPp administration (Fig. 1B). For this experiment, three experimental groups were included: the first group of mice (n = 5) received 1 MPTPp administration; the second (n = 5) received 3 MPTPp administrations; and the third (n = 5) received VEH. All three groups were monitored with [^{18}F]-FP-CIT and then *sacrificed by transcardial perfusion, and brains were collected for post-mortem immunohistochemical analysis* (Fig. 1B).

2.4. PET data acquisition, reconstruction, and quantification

PET and CT acquisitions were performed using β-cube® and X-cube®, respectively (Molecubes, Ghent, Belgium). For CT acquisition, animals were placed prone on the X-cube bed (examination duration, 4 min; X-ray beam duration, 90 s; kVp, 40; current, 400 μA; rotation time,

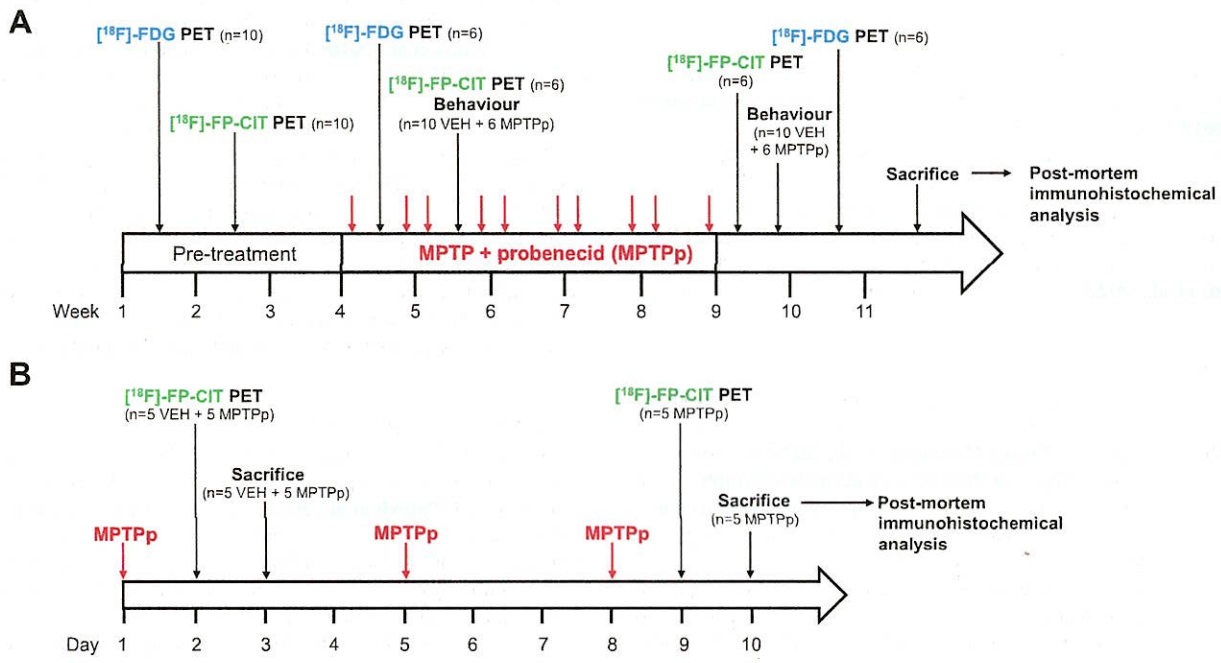

Fig. 1. (A) MPTPp treatment protocol and monitoring of mice (10 in pre-treatment and 6 in MPTPp) included in the longitudinal study. Mice exposed to MPTPp were monitored *via* PET-CT employing the 2 different radiotracers, namely [^{18}F]-FDG and [^{18}F]-FP-CIT, both before treatments and at different time points after MPTPp treatment. Behavioural observation was also performed twice (Behaviour). (B) MPTPp treatment protocol and monitoring of animals included in the second DAT binding study. MPTPp- and vehicle (VEH)-treated mice (n = 5/group) were monitored with [^{18}F]-FP-CIT after either 1 or 3 administrations, as indicated by black arrows.

60 s; angular views, 960). At the end of each CT acquisition, the bed was moved from the X-cube to the β-cube scanner for a 20-min PET acquisition (field of view, 130 × 72 mm; spatial resolution, 0.85 mm; sensitivity, 12.6%). During the PET-CT studies, animals were kept under gas anaesthesia (2% isoflurane in medical air) and were continually monitored for respiratory rate and maintained at a constant temperature by a heating pad. After the acquisition, CT images were all reconstructed with a 200 μm isotropic pixel size using the standard Image Space Reconstruction Algorithm, while PET images followed a graphics processing unit-based iterative ordered subset expectation maximization reconstruction with 30 iterations and 400 μm isotropic voxel size.

2.4.1. [^{18}F]-FP-CIT PET-CT

[^{18}F]-FP-CIT, a radioligand that binds DAT in the striatum, was prepared according to Lee and colleagues (Lee et al., 2007) and injected in the mouse tail vein (mean injected activity, 2.9 ± 0.6 MBq). After 60 min of radiotracer uptake (Im et al., 2013), mice underwent CT and PET acquisition under gas anaesthesia (2% isoflurane in medical air), as described above. PET and CT images were automatically co-registered with the Molecubes software. The resulting images were normalized by dividing them voxel by voxel by the mean tracer uptake of a control region where DAT is not expressed (*i.e.* occipital cortex) using PMOD 4.1 software (Zurich, Switzerland) and then quantified using Statistical Parametric Mapping software (SPM-12) tools (https://www.fil.ion.ucl.ac.uk/spm/software/). Specifically, PET-CT images were normalized to a home-made mouse brain atlas, based on the "Allen Reference Atlas" (https://atlas.brain-map.org/) (Presotto et al., 2022) and the mean radioactivity values for the volumes of interest for the dorsal and ventral striatum were extracted. It is essential to specify that in *in vivo* neuroimaging analysis, the reference Atlas is "Allen Reference Atlas" (https://atlas.brain-map.org/), where the striatum is identified as "dorsal striatum" and "ventral striatum". In contrast, the reference Atlas for immunohistochemistry is "The Mouse Brain in Stereotaxic Coordinates" Atlas (Franklin and Paxinos, 2008), where the total striatum corresponds to Allen's dorsal striatum, whereas the nucleus accumbens corresponds to the Allen's ventral striatum (see Supplementary Fig. 1 for a visual comparison).

2.4.2. [^{18}F]-FDG PET-CT

[^{18}F]-FDG, a widely used radiotracer that gives a measurement of glucose metabolism, was prepared for clinical use (*European pharmacopoeia*, 2013). Animals were food-deprived for 12 h prior to the experiment and injected in the tail vein with an average of 3.7 ± 0.3 MBq of [^{18}F]-FDG. After 60 min of uptake, animals underwent CT and PET acquisition under gas anaesthesia (Bascuñana et al., 2019; Shimoji et al., 2004). Then, the regional mean radioactivity values were extracted for each region in SPM-12 by applying the same atlas used for [^{18}F]-FP-CIT (Presotto et al., 2022) and they were normalized by the global mean uptake.

2.4.3. Metabolic connectivity

[^{18}F]-FDG PET regional values (part of the nigrostriatal circuit) were also analysed by applying a covariance analysis method to assess brain metabolic connectivity (Tassan Mazzocco et al., 2023) by using the brainGraph toolbox (https://github.com/cwatson/brainGraph) in R Studio software (RStudio, PBC, Boston, MA, http://www.rstudio.com/). Spearman's correlation coefficient (ρ) was calculated for each pair of regional [^{18}F]-FDG uptake values and a correlation matrix was obtained for each time point. On the light of the small sample size this last part of the analysis was performed including a region subset *i.e.* dorsal and ventral striatum, thalamus, midbrain and cortex, the latter further divided into motor and sensory aspects. Region's selection was performed considering the most relevant PD-related areas and the spatial resolution capabilities of PET tomographs designed for small animal evaluations. To statistically compare each correlation coefficient between different time points, we performed a Z test (Tassan Mazzocco et al., 2023).

2.5. Locomotor behaviour tests

The mice of the longitudinal study, receiving subchronic MPTPp treatment and PET-CT scanning (n = 6) underwent open-field testing within 1–2 days after the 3rd and 10th administration and compared with VEH-treated control mice (n = 10) (Fig. 1A). The objective was to evaluate the possible locomotor impairments resulting from MPTPp treatment in relation to *in vivo* and post-mortem marker modifications.

For this purpose, mice were individually placed at the corner of an open-field arena (50 × 50 × 30 cm) and allowed to explore the environment for 30 min, while they were recorded with a camera from above. After each session, mice were put back in their home cage, and the arena was cleaned with a 70% alcohol solution and dried with a paper towel. Videotrack software (View Point Life Science) was used for the measurement of the total distance travelled by the animals in the arena.

2.6. Immunohistochemical analyses

2.6.1. Tissue preparation

On the day of sacrifice (for details see Fig. 1), mice were deeply anaesthetized with 1.7% tribromoethanol solution (20 μl/mg, i.p) and transcardially perfused with ice-cold saline (NaCl, 0.9%) followed by 4% paraformaldehyde (PFA) in 0.1 M phosphate buffer (PB, pH 7.4). Subsequently, their brains were isolated, post-fixed in 4% PFA for 2 h, and preserved in PB saline 1× (PBS) plus 0.05% sodium azide at 4 °C. Thereafter, brains were coronally cut on a vibratome to obtain sections (40 μm) for immunohistochemical processing.

For each animal, we collected 3 coronal sections according to the following stereotaxic coordinates: A) striatum, 1.34 to 0.74 mm; B) SNc, −2.92 to −3.52 mm relative to bregma, accordingly to the mouse brain atlas (Franklin and Paxinos, 2008).

2.6.2. TH immunohistochemistry

For immunohistochemical detection of TH in the total striatum and SNc, we applied the diaminobenzidine (DAB) technique, as previously described (Pinna et al., 2016). Briefly, free-floating sections were rinsed in PBS 1×, incubated with 1% H_2O_2 (30% v/v, Merck) in PBS (10 min at room temperature [RT]), blocked and permeabilized with 5% normal goat serum (NGS) plus 0.1% Triton X-100 (20 min at RT), and then incubated with primary antibody directed toward TH (polyclonal rabbit anti-TH, 1:1000, AB152, Millipore Corporation, Billerica, MA, USA) (2 nights at RT). Thereafter, sections were incubated with the biotinylated secondary antibody (goat anti-rabbit; 1:500, Vector, Peterborough, UK) (1 h at RT), then the avidin–peroxidase protocol (ABC, Vector, Peterborough, UK) was applied for visualization, using 3,3′-diaminobenzidine (Merck) as a chromogen. Afterwards, sections were mounted onto super-frost glass slides, dehydrated, and coverslipped using Eukitt® mounting medium.

2.6.3. DAT immunofluorescence

For immunohistochemical detection of DAT in the total striatum and nucleus accumbens, we applied a previously validated immunofluorescence protocol (Parekh et al., 2022). Free-floating sections were rinsed in PB 0.1 M, blocked, and permeabilized in 3% NGS, and 0.3% Triton X-100 in PB (3 h at RT), and then incubated in the same solution with the primary antibody (monoclonal rat anti-DAT; 1:1000, MAB369, Millipore Corporation, Billerica, MA, USA) (2 nights, 4 °C). Then, sections were rinsed, and incubated with the biotinylated secondary antibody (biotinylated goat anti-rat; 1:200) (2 h at RT), followed by incubation with AlexaFlour® 488-labelled streptavidin (1:500, Jackson ImmunoResearch Europe, Newmarket, UK) (1 h at RT). Afterward, sections were rinsed in PB 0.1 M and mounted onto super-frost glass slides using Mowiol® mounting medium. Omission of either the primary or

secondary antibodies served as a negative control and yielded no labelling (data not shown).

2.6.4. TH and DAT acquisition and analysis in the SNc and striatum

Stereological analysis of the total number of TH-positive neurons in the SNc was carried out, as previously described, using the software Stereologer (Casu et al., 2004; Costa et al., 2019).

For the acquisition of TH immunostaining in the striatum, images of a single wavelength (8-bit depth) were obtained with a high-resolution scanner for medical slides (Super Coolscan 9000ED, Nikon) set at 4000 dpi (Pisanu et al., 2015).

For the acquisition of DAT immunofluorescence in the striatum, images of a single wavelength (14-bit depth) were obtained with the ZEISS Axio Scan Z1 slide scanner (Zeiss, Germany) connected to the Axiocam 506 digital camera (fluorescence imaging, 2752 × 2208 pixels, Zeiss, Germany), and equipped with the light-emitting diode light source Colibri 2.

For the analysis, all images were background subtracted, and the densities of immunoreactive TH- and DAT-positive fibres were determined quantitatively by measuring the mean grey density in fixed regions representing the total striatum through the ImageJ software (U.S. National Institutes of Health, Bethesda, MD, USA). The final values were expressed as a percentage of the VEH-treated control group.

2.7. Statistical analysis

Statistical analysis was performed using Prism 8 (GraphPad Software Inc., La Jolla, CA, USA). Given the small sample size and the deviation from normality of our data, we employed non-parametric statistical tests. In particular, the Friedman test followed by Dunn's *post hoc* multiple comparison test was applied when testing differences among repeated measures (longitudinal study) and Kruskal–Wallis test followed by Dunn's *post hoc* multiple comparison test for independent groups (DAT and TH immunoreactivity, early DAT binding study). The Mann–Whitney test was then applied to test the differences between 2 unpaired groups. Finally, the correlation between DAT binding values measured *in vivo* and DAT and TH immunoreactivity values measured by immunohistochemistry was assessed using Pearson's correlation test. Statistical significance was accepted at $p < 0.05$.

3. Results

3.1. [^{18}F]-FP-CIT and [^{18}F]-FDG uptake: longitudinal study

In the longitudinal study, a significant decrease in [^{18}F]-FP-CIT uptake in the dorsal striatum of mice was observed after 10 MPTPp administrations, compared with values before treatment ($p = 0.0418$). However, a trend of [^{18}F]-FP-CIT uptake reduction was already observed after 3 MPTPp administrations compared with values before treatment (Fig. 2B; $p = 0.0866$), as also highlighted by the PET-CT-DAT representative images shown in Fig. 2A. Conversely, no significant difference was observed in the ventral striatum (Fig. 2B; $p > 0.05$).

[^{18}F]-FDG uptake was significantly decreased in the dorsal striatum (Fig. 2C; pre-MPTPp *vs* MPTPp 1 administration, $p = 0.0078$; pre-MPTPp *vs* MPTPp 10 administrations, $p = 0.0418$) and ventral striatum of animals that received 1 and 10 MPTPp administrations (Fig. 2C; pre-MPTPp *vs* MPTPp 1 administration, $p = 0.0187$; pre-MPTPp *vs* MPTPp 10 administrations, $p = 0.0187$) compared with values before treatment. A similar result was also detected in the thalamus, where [^{18}F]-FDG uptake was significantly reduced after both 1 ($p = 0.0078$) and 10 MPTPp administrations ($p = 0.0418$) and in the somatomotor areas where [^{18}F]-FDG uptake was significantly reduced after 1 administration ($p = 0.0187$), compared with values before treatment (Fig. 2C).

Since significant differences in [^{18}F]-FDG uptake were already

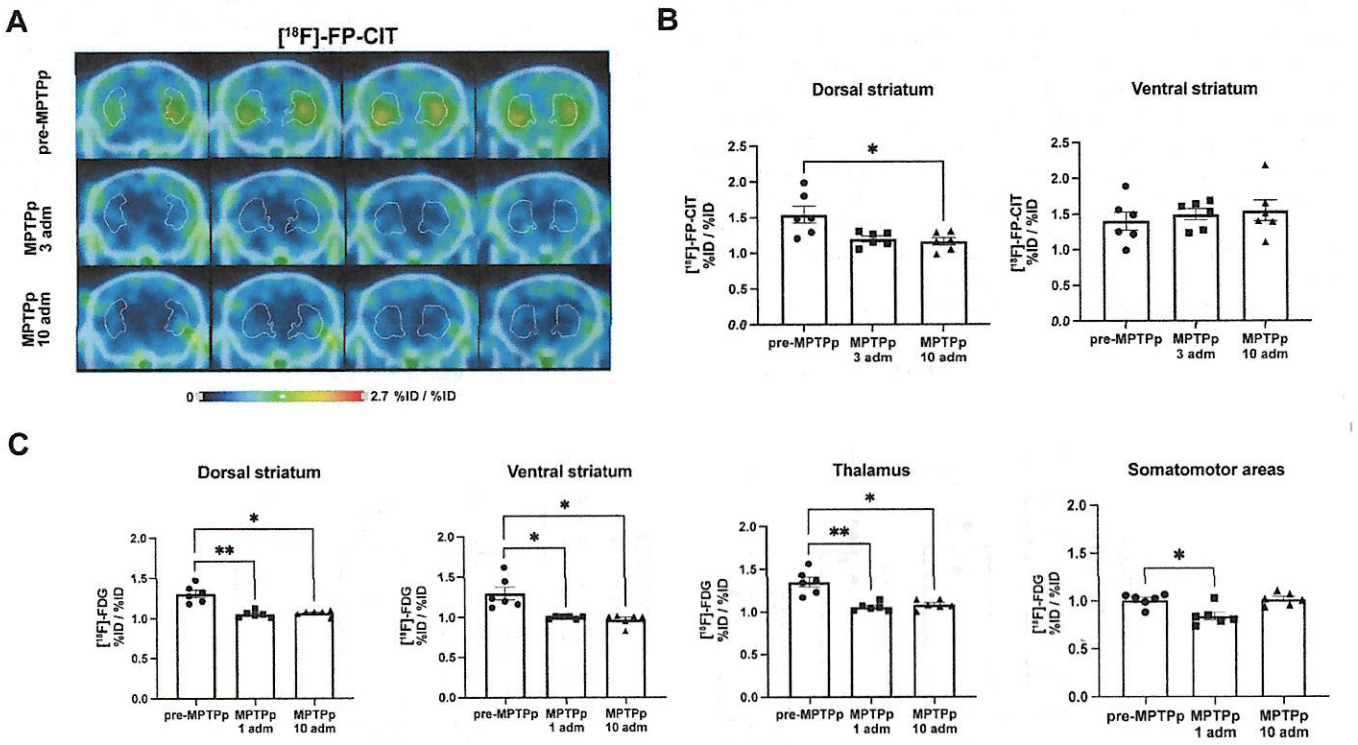

Fig. 2. Representative PET-CT images showing striatal [^{18}F]-FP-CIT uptake before treatment and after 3 and 10 MPTPp administrations (adm), where white contouring represents the volume of interest of the dorsal striatum used for quantification (A). [^{18}F]-FP-CIT uptake in the dorsal and ventral striatum of C57BL/6J mice, both before treatment and after 3 or 10 administrations of MPTPp ($n = 6$/group), expressed as ratio to the occipital cortex (%ID/%ID) (B). [^{18}F]-FDG regional uptake in selected brain regions of MPTPp mice before treatment and after 1 and 10 MPTPp administrations expressed as ratio to the total brain (%ID/%ID) ($n = 6$/group) (C). Friedman test followed by Dunn's *post hoc* multiple comparison test: *$p < 0.05$, **$p < 0.01$. Data are plotted as mean ± standard error of the mean.

detectable after the first MPTPp administration, we proceeded to replicate the [^{18}F]-FP-CIT study at earlier time points (1 and 3 administrations) in a separate cohort of mice. PET-CT-DAT image quantification in 3 independent groups of mice, namely, the VEH group ($n = 5$), the group receiving 1 administration of MPTPp (n = 5), and the group receiving 3 administrations of MPTPp (n = 5), resulted in a significant [^{18}F]-FP-CIT uptake decrease in the dorsal striatum after 3 (Fig. 3; $p = 0.0308$), but not after 1, MPTPp administration (Fig. 3; $p > 0.05$), compared with VEH-treated animals confirming the trend observed for the longitudinal study. No significant difference in the three groups was found in the ventral striatum (Fig. 3; $p > 0.05$).

3.2. Behavioural evaluation

The open-field test, performed on the MPTPp-treated mice subjected to PET-CT imaging (longitudinal study) resulted in a significant increase in the total distance travelled by mice receiving 10 MPTPp administrations compared with those receiving VEH (Fig. 4B; $p = 0.0312$). Conversely, no difference was observed between VEH- and MPTPp-treated mice receiving 3 administrations (Fig. 4A; $p > 0.05$).

3.3. TH and DAT immunoreactivity upon completion of MPTPp treatment

Considering the progressive reduction in [^{18}F]-FP-CIT uptake observed in the dorsal striatum of living MPTPp-treated mice, we next asked whether, in the same mice, these alterations were associated with changes in the protein content of TH and DAT, two established markers used to evaluate the synthesis capacity of dopamine and the functionality of dopaminergic terminals, respectively.

The measurement of TH immunoreactivity in the total striatum and SNc, alongside the assessment of DAT immunoreactivity in the striatum, was conducted *ex vivo* in the mice involved in both experiments illustrated in Fig. 1.

For immunoreactivity of TH in the total striatum, the Kruskal–Wallis test revealed a main effect of MPTPp treatment (Fig. 5B; $p = 0.0372$). Dunn's *post hoc* multiple comparisons test highlighted a significant difference in the density of striatal TH-positive fibres in mice receiving 3 administrations of MPTPp compared with VEH-treated mice (Fig. 5B; $p = 0.0424$). On the other hand, mice receiving 1 administration of MPTPp showed only a trend toward a decrease in TH-immunoreactivity compared with VEH-treated mice (Fig. 5B; $p = 0.1024$). Notably, the Mann–Whitney test revealed a net reduction in the density of striatal TH-positive fibres of mice receiving 10 injections of MPTPp compared with VEH-treated mice (Fig. 5C; $p = 0.0019$).

For immunoreactivity of TH in the SNc, the Kruskal–Wallis test indicated a main effect of MPTPp treatment (Fig. 5D; $p = 0.0478$). We found a significant reduction in the total number of TH-positive neurons in the SNc of mice receiving 3 administrations of MPTPp (Fig. 5D; $p = 0.0392$), but not 1 administration (Fig. 5D; $p = 0.2691$), compared with mice treated with VEH. In addition, the Mann–Whitney test revealed a net reduction in the total number of TH-positive neurons in the SNc of mice receiving 10 administrations of MPTPp compared with mice treated with VEH (Fig. 5E; $p = 0.0043$).

For DAT in the total striatum, the Kruskal–Wallis test revealed a main effect of MPTPp treatment (Fig. 6B; $p = 0.005$). Specifically, Dunn's *post hoc* multiple comparisons test found a significant difference in the density of striatal DAT-positive fibres in mice receiving 3 administrations (Fig. 6B; $p = 0.0473$), but not 1 administration (Fig. 6B; $p > 0.05$), of MPTPp compared with mice treated with VEH. In addition, the Mann–Whitney test revealed a marked reduction in the density of striatal DAT-positive fibres of mice receiving 10 administrations of MPTPp compared with VEH (Fig. 6C; $p = 0.0017$).

For DAT in the nucleus accumbens of mice receiving either 1 or 3 administrations, the Kruskal–Wallis test did not reveal any effects of MPTPp treatment (Fig. 6D; $p = 0.6200$). Conversely, the Mann–Whitney test revealed a marked reduction in the density of accumbal DAT-positive fibres of mice receiving 10 administrations of MPTPp compared with VEH (Fig. 6E; $p = 0.0010$).

Overall, and in line with the [^{18}F]-FP-CIT results, these data highlight that, excluding the time points of 1 and 3 administrations in the nucleus accumbens, repeated MPTPp treatment elicits progressive neurotoxic effects affecting striatal dopaminergic terminals, which are detectable starting from the third administration of MPTPp.

3.4. Correlation between in vivo PET imaging and post-mortem immunohistochemistry data

Next, we conducted a correlation analysis between *in vivo* [^{18}F]-FP-CIT imaging and *ex vivo* DAT immunohistochemical measurements obtained in the same MPTPp-treated mice across all time points. In the dorsal striatum, Pearson's correlation test revealed a strong positive linear association (Fig. 7A; $p = 0.0089$). We observed a similar tendency in the ventral striatum, although it was not significant (Fig. 7B; $p = 0.0509$). We also correlated *in vivo* [^{18}F]-FP-CIT data with the density of *ex-vivo* TH-positive fibres in the dorsal striatum and found a tendency toward a significant positive correlation (Fig. 7C; $p = 0.0539$). Finally, the values of [^{18}F]-FP-CIT in the dorsal striatum did not correlate with the number of *ex-vivo* TH-positive neurons in the SNc (Fig. 7D; $p > 0.05$).

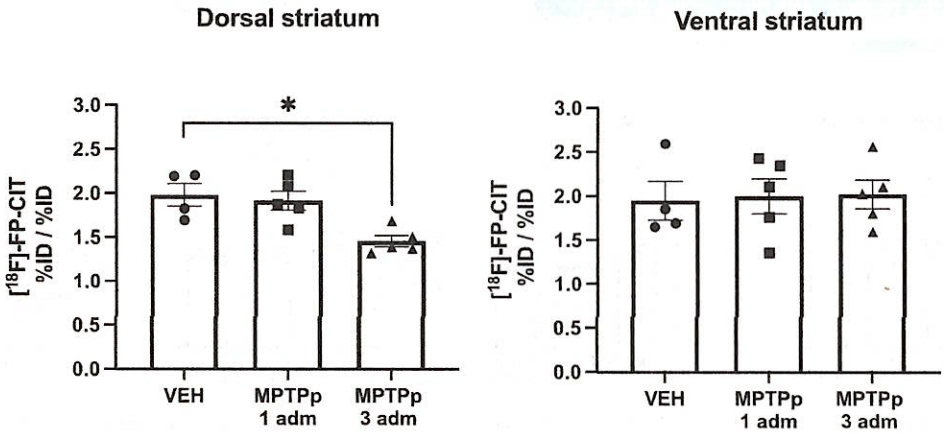

Fig. 3. Striatal [^{18}F]-FP-CIT uptake quantification in the MPTPp mouse. Bar graphs showing [^{18}F]-FP-CIT uptake quantification, expressed as ratio to the occipital cortex (%ID/%ID), in the dorsal and ventral striatum of independent groups of mice receiving the vehicle (VEH), or either 1 or 3 administrations (adm) of MPTPp (n = 5/group). Friedman test followed by Dunn's *post hoc* multiple comparison test: $^*p < 0.05$. Data are plotted as mean ± standard error of the mean.

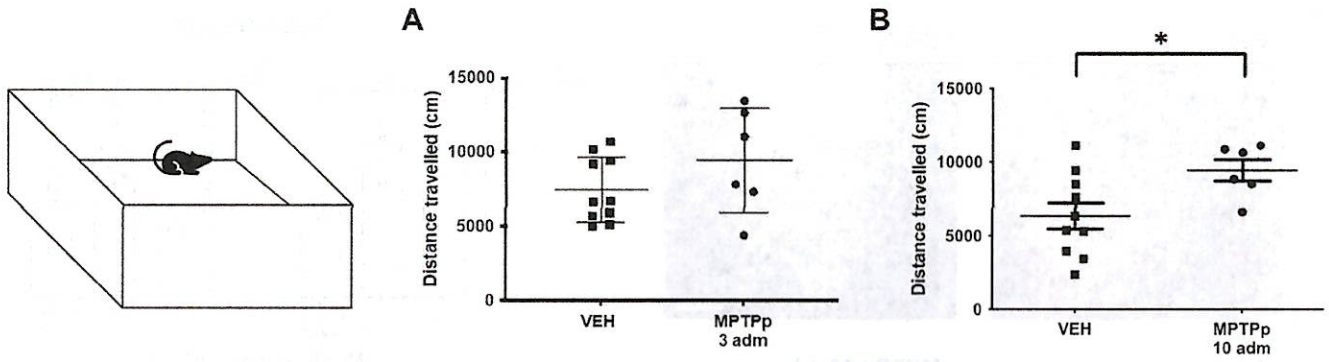

Fig. 4. Open-field test was performed in MPTPp mice. Graphs showing the distance travelled by vehicle (VEH, $n = 10$)- and MPTPp-treated mice receiving either 3 (A) or 10 (B) administrations (adm; n = 6) when exposed to an open field arena for 30 min. Mann–Whitney test: $^{*}p < 0.05$. Data are plotted as mean ± standard error of the mean.

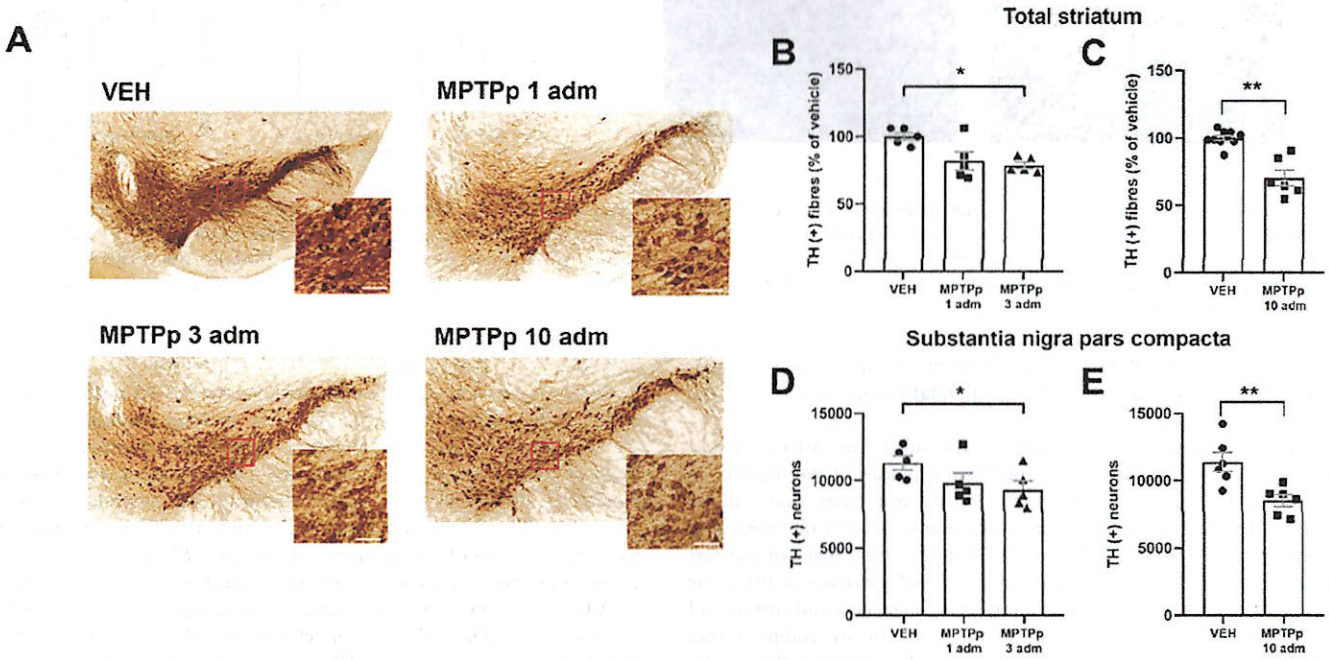

Fig. 5. Representative images of the substantia nigra pars compacta (SNc) immunostained for tyrosine hydroxylase (TH) (A). Bar graphs showing the density of TH-positive fibres in the total striatum (B-C), and the total number of TH-positive neurons in the SNc (D-E) of mice treated with either the vehicle (VEH) or 1, 3, or 10 administrations (adm) of MPTPp. (B, D) Kruskal–Wallis test followed by Dunn's *post hoc* multiple comparison test: $^{*}p < 0.05$. (C, E) Non-parametric Mann–Whitney test: $^{**}p < 0.01$. *Scale bar = 50 μm. Data are plotted as mean ± standard error of the mean.*

3.5. Metabolic connectivity

In the condition before treatment (baseline), the correlation matrix derived by [^{18}F]-FDG PET scans showed a pattern of strong positive correlation among cortical regions, as well as among subcortical regions. The midbrain, instead, only showed weak non-significant ($p > 0.05$) negative correlations with the other brain regions (Fig. 8A).

Already after 1 MPTPp administration, we observed the loss of significant correlation between the dorsal and ventral parts of the striatum. The dorsal and ventral portions of the striatum displayed a different pattern of connectivity from each other, since following 1 MPTPp administration, the ventral striatum lost all the connections with other brain regions, while in the dorsal striatum a positive correlation with the thalamus and midbrain was observed. When comparing pre-MPTPp and 1 MPTPp administration, we found significant differences in the correlation coefficients of midbrain *versus* thalamus and dorsal striatum (Fig. 8B).

After 10 MPTPp administrations, all of the significant inter-regional correlations were lost, except for the somatomotor areas, which positively correlated with the midbrain and negatively correlated with the ventral striatum (Fig. 8A). Similarly, the midbrain maintained the negative correlation with the ventral striatum (Fig. 8A). As a matter of fact, the connection between the dorsal and the ventral part of the striatum was found to be significantly different from that observed before treatment (Fig. 8B). Moreover, after 10 MPTPp administrations, we found a significant difference in the connection between somatomotor cortical areas and ventral striatum and midbrain, and between thalamus and ventral striatum, compared with values before treatment (Fig. 8B).

4. Discussion

The primary objective of the present research work was to study and compare *in vivo* PET imaging and post-mortem immunohistochemistry

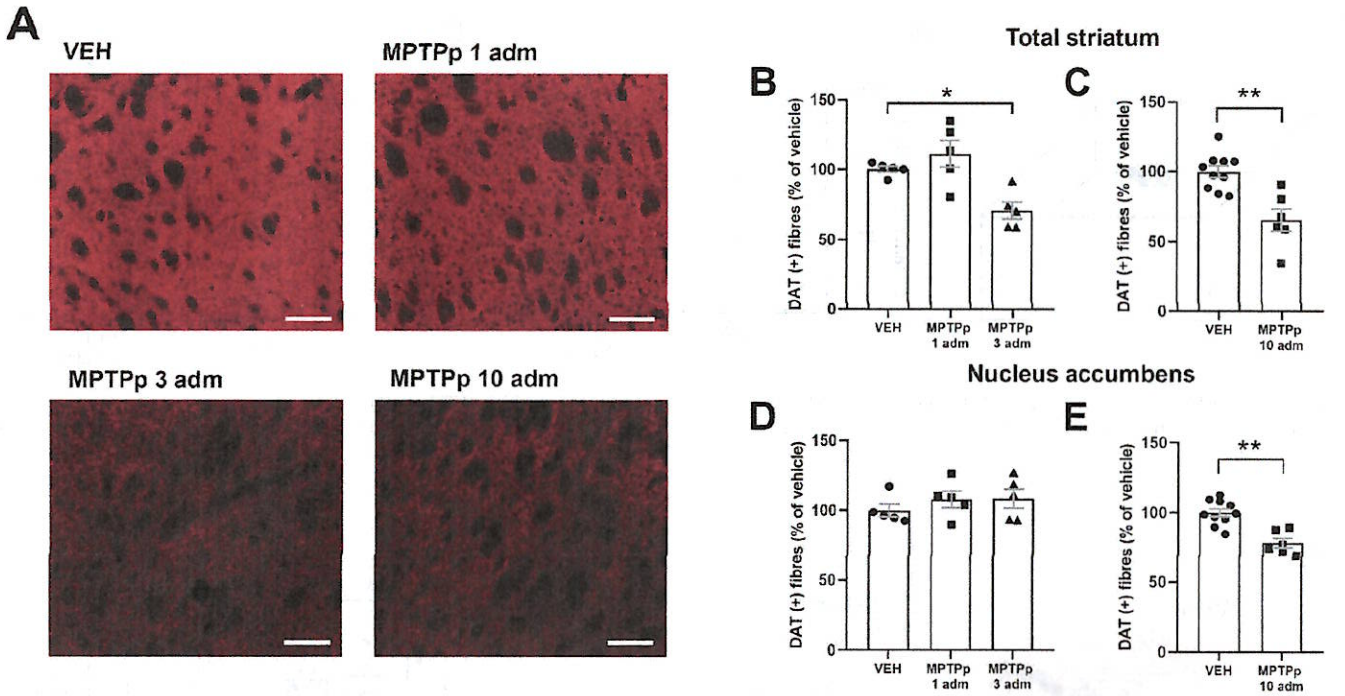

Fig. 6. Representative images of the total striatum immunostained for the dopamine transporter (DAT) (A). Bar graphs showing the density of DAT-positive fibres in the total striatum of mice treated with either the vehicle (VEH) or 1, 3, or 10 administrations (adm) of MPTPp (B-C). Bar graphs showing the density of DAT-positive fibres in the nucleus accumbens of mice treated with either the vehicle (VEH) or 1, 3, or 10 administrations (adm) of MPTPp (D-E). (B-D) Kruskal–Wallis test followed by Dunn's *post hoc* multiple comparison test: *$p < 0.05$. (C-E) Non-parametric Mann–Whitney test: **$p < 0.01$. Scale bar = 100 μm. Data are plotted as mean ± standard error of the mean.

to investigate in MPTPp-treated mice the progressive timing of dopamine denervation, thus providing a relationship between these variables.

To this aim, we took advantage of the subchronic MPTPp mouse model of PD, which mirrors the prodromal phases of the disease, to identify early biomarkers indicative of disease onset that can be employed both in clinical settings, to enhance patient diagnosis and treatment, and in preclinical studies to test new drugs that can contrast neurodegeneration. Clinical manifestations and diagnosis of PD occur when the denervation of dopaminergic SNc neurons is advanced and most of the dopamine terminals in the striatum are compromised, impairing therapy efficacy. For this reason, the understanding of the modifications occurring in preclinical models that mirror the prodromal stages of PD is fundamental in the pursuit of new strategies for both diagnostic and interventional approaches, which might prevent or delay the progression of PD.

Several animal models have been developed in mammals to reproduce and study PD pathophysiology that can be generated either through neurotoxin administration, genetic modifications, or α-synuclein propagation (Becker et al., 2021). Neurotoxin-based models, such as MPTP, 6-hydroxydopamine, and rotenone, display a phenotype characterized by clear nigrostriatal neurodegeneration, recapitulating the motor effects typical of the advanced disease (Bezard et al., 2013; Blandini and Armentero, 2012). However, certain models can be extended to investigate prodromal PD signs. One such model is the subchronic MPTPp mouse model, which unlike acute models based on the administration of elevated doses of MPTP, allows a gradual and progressive degeneration of nigrostriatal dopaminergic neurons and terminals (Petroske et al., 2001; Taguchi et al., 2020), detectable for up to 6 months following treatment cessation (Petroske et al., 2001). Importantly, depending on the combined dose of MPTP and probenecid used, mice subjected to subchronic MPTPp treatment may show significant dopamine denervation, without the evident manifestation of motor impairments (Baranyi et al., 2016; Serra et al., 2023).

Using this model, we have evaluated, *in vivo* PET-CT radiotracers to detect both signs of dopaminergic nerve endings deterioration and modification in glucose metabolism as markers of connectivity in the brain of treated mice. Concurrently with neuroimaging analyses, we monitored, by *ex vivo* immunohistochemistry, the neurodegenerative progression of nigrostriatal dopaminergic neurons by employing stereological analysis of TH-positive neurons in the SNc and density analysis of DAT and TH-positive dopaminergic terminals in the striatum.

Albeit in a small cohort of animals, where type 2 errors cannot be excluded particularly when the effect size is small, our results showed that, in mice, the subchronic MPTPp treatment produced a progressive reduction in [^{18}F]-FP-CIT uptake in the dorsal, but not the ventral, portion of the striatum. Moreover, while 1 administration of MPTPp did not exert any detectable effect, either 3 or 10 MPTPp administrations produced a significant decay in [^{18}F]-FP-CIT uptake in the dorsal striatum. These findings are consistent with previous PET investigations that examined dopamine uptake and residual DAT binding in early diagnosed patients with PD (Ishibashi et al., 2014; Kerstens et al., 2023). The absence of DAT binding loss in the ventral striatum is also consistent with previous clinical evidence, indicating a minor involvement of this area in the early stages of PD (Brooks, 2016).

Interestingly, in the present study, and for the first time in the subchronic MPTPp-mouse model of PD, we found a clear positive correlation between PET-CT analysis and *ex vivo* data at different time points, supporting the importance of the use of PET-CT analysis as a predictive method for the early diagnosis of PD. At the same time, these results confirm the validity of the progressive MPTPp mouse model for the evaluation of prospective neuroprotective drugs in PD. Indeed, the decrease in [^{18}F]-FP-CIT uptake in mice receiving either 3 or 10 MPTPp administrations was accompanied by a loss in DAT-positive fibres measured post-mortem in the dorsal striatum, as highlighted by the positive linear association observed between values.

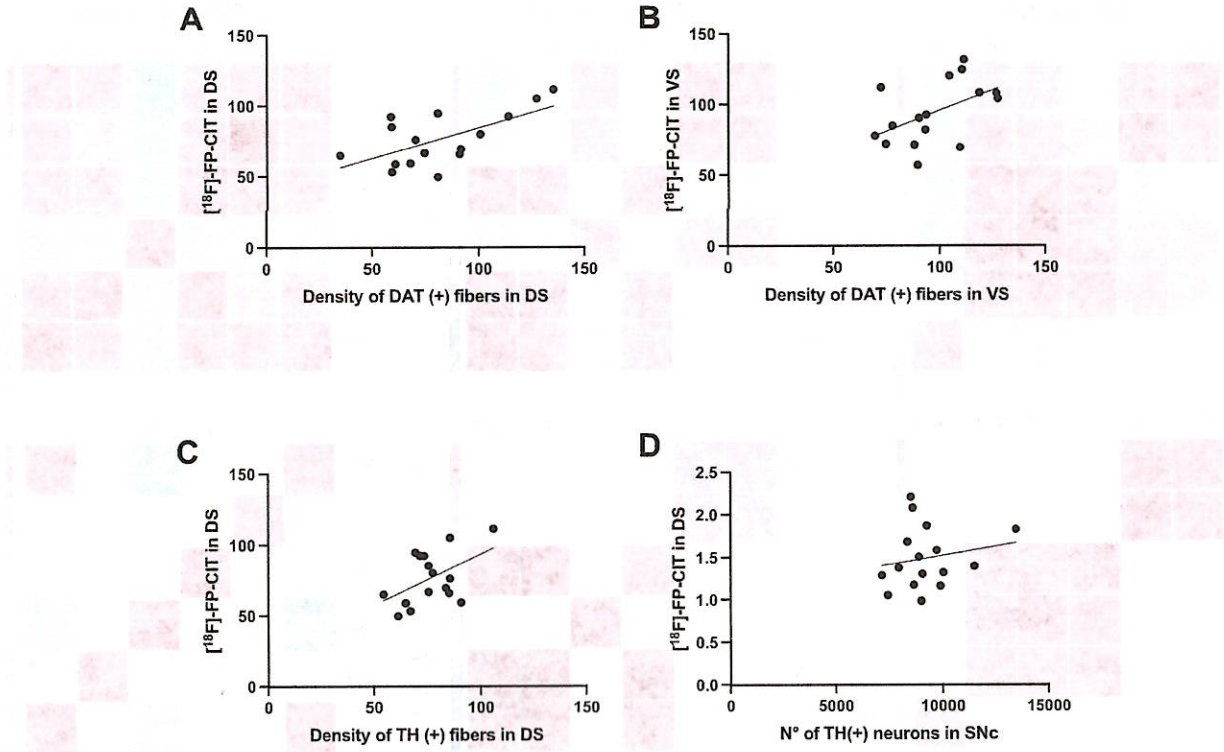

Fig. 7. Correlation between *in vivo* dopamine transporter (DAT) ([^{18}F]-FP-CIT uptake values) and *ex vivo* density of DAT- (A,B) and tyrosine hydroxylase (TH)-positive fibres in the striatum (C) and number of TH-positive neurons in SNc (D), expressed either as a percentage of vehicle (VEH) (A-C) or number of neurons (D). A) Correlation between [^{18}F]-FP-CIT uptake and *ex vivo* DAT fibre density in the dorsal striatum showed a strong positive linear association ($r = 0.6298$, $p = 0.0089$). B) Correlation between [^{18}F]-FP-CIT uptake and *ex vivo* DAT fibre density in the ventral striatum showed a tendency of positive association ($r = 0.4956$, $p = 0.0509$). C) Correlation between [^{18}F]-FP-CIT uptake and *ex vivo* TH fibre density in the dorsal striatum showed a tendency of positive association ($r = 0.4901$, $p = 0.0539$). D) Correlation between [^{18}F]-FP-CIT uptake in the dorsal striatum and *ex vivo* number of TH-positive neurons in the substantia nigra pars compacta (SNc) showed no association ($r = 0.1854$, $p > 0.05$).

Furthermore, the results were substantiated through *ex vivo* stereological analyses, where we observed a substantial and progressive reduction in the number of TH-positive neurons in the SNc and in the density of TH-positive fibres in the total striatum. These changes were observed starting from the third administration of MPTPp and slowly increase, until the tenth administration of MPTPp in the SNc and the striatum of MPTP-treated mice, respectively. On the other hand, no reduction of TH-positive neurons in the SNc and a non-significant trend toward a decrease in TH-immunoreactivity in the striatum was detected after the first administration of MPTP. These data are consistent with previous studies that demonstrated the progression of nigrostriatal degeneration in this subchronic MPTPp model of PD (Baranyi et al., 2016; Petroske et al., 2001; Schintu et al., 2009; Serra et al., 2023). Of note, TH-positive fibres in the total striatum, but not TH-positive neurons in the SNc, were positively correlated with *in vivo* DAT binding, confirming that nigral damages *per se* do not fully explain striatal modifications (Grosch et al., 2016). These findings are in line with other results indicating a lack of association between residual neurons in the SN and damage at synaptic striatal terminal (Gaspar et al., 1983; Kordower et al., 2013).

Of great importance, the lack of correlation found between [^{18}F]-FP-CIT values in the dorsal striatum *vs* the number of TH-positive neurons in the SNc may hold significant translational implications since a cross-sectional post-mortem study showed that, at the onset of the symptoms, approximately 30% of nigral dopaminergic neurons are lost, with the loss of striatal dopamine terminals accounting for about 70% (Cheng et al., 2010). Moreover, dopaminergic fibre density in the dorsal putamen of PD patients exhibited a rapid and substantial decline, culminating in near-complete loss four years post-clinical diagnosis, whereas TH-positive neurons in SNc were less severely affected, resulting in a residual dopaminergic neuronal population which can be detected even decades after the initial diagnosis (Kordower et al., 2013).

Finally, using [^{18}F]-AV-1451, a radiopharmaceutical that labels neuromelanin in the midbrain as a surrogate imaging marker of pigmented dopamine neurons in the SNc, Hansen and colleagues found no correlation between nigral signal and striatal DAT binding (Hansen et al., 2016). As previously stated, in our study we observed an effect of MPTPp on DAT only after 3 administrations with a slow and not significant decline thereafter with approximately a 35% reduction of striatal markers lower than that described at motor sign comparison in patients. At this clinical stage PET imaging studies showed the highest reduction of dopaminergic synaptic markers in the dorsal putamen contralateral to the body side with the highest motor impairment, that slowly decline along disease progression. On the contrary, in the less affected regions a rapid decline was still present (Kerstens et al., 2023; Nandhagopal et al., 2009). This may suggest that our model mimics the prodromal PD in the temporal frame that precedes the third administration of MPTPp and an early phase of the disease preceding the motor impairment during the last time frame.

In contrast to DAT binding measured by [^{18}F]-FP-CIT, [^{18}F]-FDG uptake significantly decreased in the dorsal striatum already from the first MPTPp administration, proving to be an earlier marker than DAT in detecting alterations in neuronal function preceding the degeneration of nigrostriatal neurons. In fact, it is known that functional alterations often precede structural changes in the brain. Of note, [^{18}F]-FDG uptake decrease was extended to the ventral striatum, thalamus and, starting from the third MPTPp injection, to somatomotor cortical regions. A Parkinson's Disease Related Pattern (PDRP) has been described by several groups for PD patients. Differently from what we observed, in patient's studies, the FDG-PET pattern is characterized by

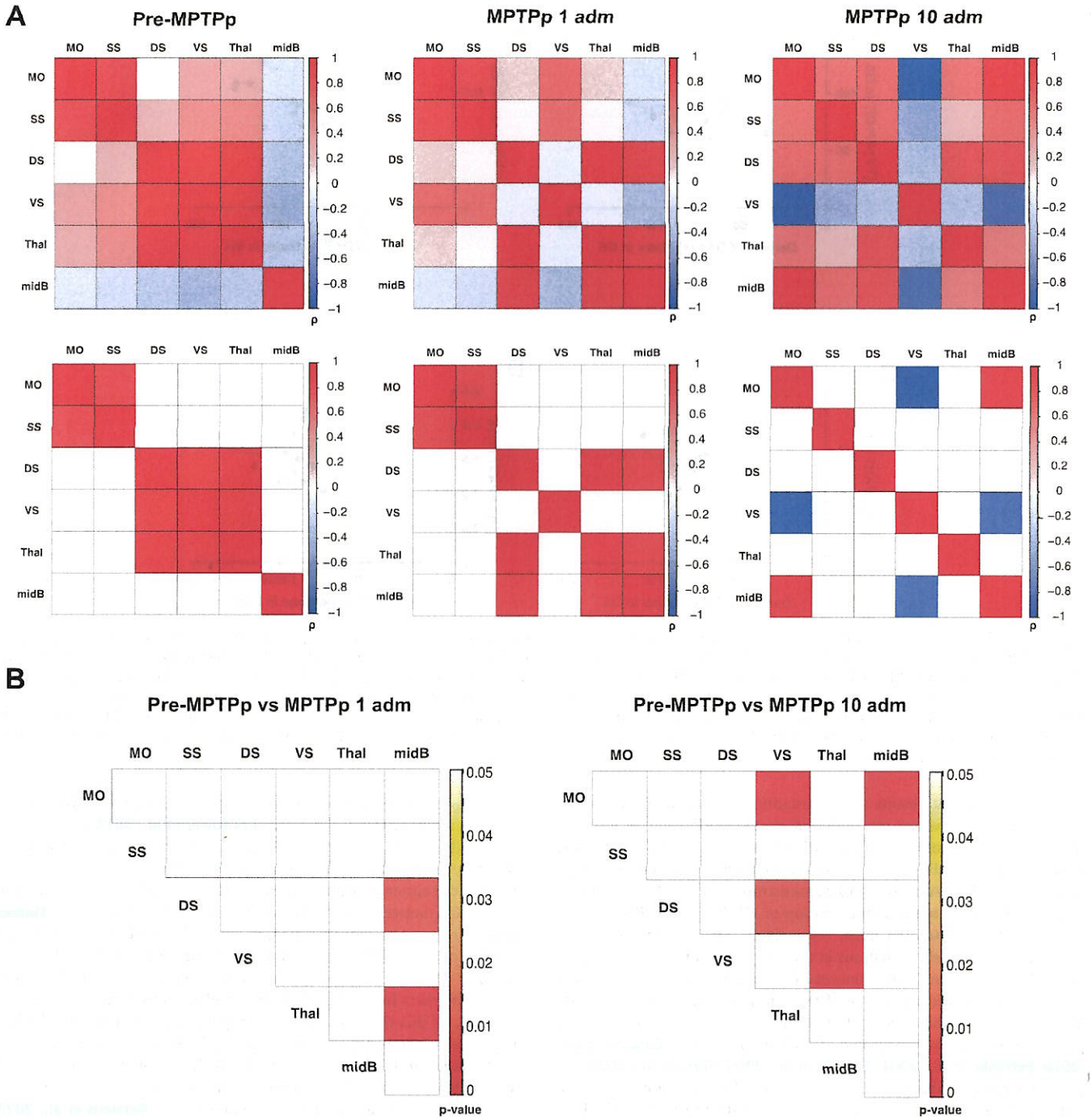

Fig. 8. [^{18}F]-FDG PET correlation matrices of pre-MPTP, 1 MPTPp administration (adm) and 10 MPTPp adm (above) and the same matrices showing significant ($p < 0.05$) correlations only (below), where red squares represent positive correlation coefficients (ρ) and blue squares represent negative correlation coefficients (A). Correlation matrices are statistically compared between groups (pre-MPTPp *vs* MPTPp 1 adm and pre-MPTPp *vs* MPTPp 10 adm) and only the connections that are significantly different between the two groups ($p < 0.01$, uncorrected) are shown in the upper triangular matrix (B). DS = dorsal striatum; midB = midbrain; MO = somatomotor cortical areas; SS = somatosensory cortical areas; Thal = thalamus; *VS* = ventral striatum.

hypometabolism in parieto-occipital and premotor cortices together with a metabolic preservation or increase in cerebellum, pons, thalamus and striatal subregions (Eidelberg et al., 1994). This pattern has been correlated with H&Y stage and UPDRS motor scores, however aged-related metabolic modifications and clinical presentation represent confound variables (Matthews et al., 2018). Our study did not include aged animals and this may explain some differences between PDRP and our findings. Moreover, PDRP is mainly derived from PD patients presenting motor signs that were not the case of our model. Finally, as previously stated, at later time frames, our model likely still reflects a prodromic disease phase, anterior to the appearance of motor signs, which is poorly described in terms of imaging metabolic data.

Of particular interest for the scope of this study were the early modifications in brain connectivity. Specifically, after the first MPTPp administration, mice brain lost the correlation between the dorsal and ventral parts of the striatum, whereas the thalamus and the dorsal part of

the striatum acquired metabolic connectivity with the midbrain. After 10 administrations, almost all connectivity was lost, except for some correlations in the somatomotor cortical areas, midbrain, and ventral striatum. While additional investigations are required to establish this neuroimaging feature as a prodromal biomarker of PD, the observed positive correlation between the somatomotor cortical areas and the midbrain following 10 administrations is particularly intriguing, given the pivotal roles of these brain areas in the regulation of movements and the integration of sensory information into motor responses. Interestingly, we also observed that the dorsal and ventral striatum displayed a different connectivity pattern between each other. These results further support the importance of [^{18}F]-FDG as an early-stage marker of neurodegeneration in PD and they are consistent with a previous metabolic connectivity study performed in early PD patients, where it was observed a significant connectivity loss in the dorsal dopamine pathway (Sala et al., 2017). Similar results were observed also in a different mouse model of PD, obtained by 6-hydroxydopamine injection, where metabolic connectivity in the cortico-striatal-thalamic loop was found to be impaired (Im et al., 2016). Due to the small sample size achievable in rodent studies, we did not select a modelled approach based on principal component analysis, independent component analysis, or graph theory but a simple normalized covariance between regions analysis. In addition, for identification of network modifications, we selected a priory area known to be involved in PD and with an anatomical dimension adequate for the small resolution of animal dedicated tomographs and particularly for mouse brain. Recently, using a modified principal component analysis approach on a clinical subtypes stratified PD population of patients, a subnetwork of interconnected regions present along all stages of disease progression with additional features related to stage or disease phenotype, was described (Spetsieris and Eidelberg, 2021, 2023). Despite differences in the methodological approach between connectomics analyses and distinctions in the topographic and functional organisation of the mouse brain in comparison to that of human, the observations of authors are in line with our finding and delineate an increase of the dysfunctional network as the disease progresses.

[^{18}F]-FDG PET has been largely employed in patients for differential diagnosis of PD (Eckert et al., 2005). However, only a few studies have highlighted its usefulness in predicting PD progression starting from the prodromal or early phase of the disease that anticipate motor signs leading to inconsistencies due to the difficulty in recruiting a homogeneous cohort of prodromal patients (Carli et al., 2020; Holtbernd et al., 2014; Peng et al., 2014; Schindlbeck et al., 2020). Moreover, most of these studies are mainly focused on the identification of disease-specific metabolic covariance patterns and how they can predict conversion into PD.

Finally, we evaluated the impact of the observed neuroimaging brain alterations on the motor functions of treated mice. We chose a motor behavioural test that did not require any training to avoid interferences with the PET studies. Using this test, we observed a significant increase in locomotor activity at the end of treatment in subchronic MPTPp-treated mice compared with VEH-treated mice. This behavioural observation, which might appear counterintuitive, has been already reported using a similar subchronic MPTPp protocol (Baranyi et al., 2016; Chia et al., 1996; Meredith and Kang, 2006; Schumm et al., 2012), suggesting that MPTP may disrupt neuronal activity and connectivity in a way that produces a paradoxical increase of motility. Based on previous studies, we may hypothesize a compensatory mechanism consisting in a reduction of dopamine uptake sites in the striatum at early times after the MPTP treatment (Araki et al., 2001), or a compensatory up-regulation in dopamine D2 receptors detectable in the striatum after MPTP treatment (Tanji et al., 1999). Consistent with these mechanisms, dopamine release in unilaterally 6-hydroxydopamine lesioned rats did not decrease in the striatum until a 97% reduction in TH-immunoreactive terminals was achieved (Wang et al., 2004). Similarly, MPTP-lesioned monkeys carrying moderate dopamine denervation showed a 300% increase in endogenous striatal DA release (Perez et al., 2008), whereas this response was almost completely reduced in severely depleted monkeys (Perez et al., 2008). Although the neuroanatomical substrates underlying motor control are similar in humans and rodents, the behavioural repertoire mediated by those circuits and the ability to respond to insults are not (Luchtman et al., 2009, 2012), as suggested by the occurrence of compensatory mechanisms which may stimulate motor behaviour. Therefore, the evaluation of rodent's locomotor behaviour does not seem to offer a valuable prodromic marker that could be correlated to *in vivo* imaging or *ex vivo* immunohistochemical studies (Chia et al., 1996; Schumm et al., 2012). As stated in the introduction, the neurotoxic events in the MPTPp model are long-lasting since they can still be detected up to 6 months after withdrawal from treatment (Meredith and Rademacher, 2011; Petroske et al., 2001; Serra et al., 2023), however in the present study, evaluations were performed only at early times after MPTPp treatment and therefore the results obtained reflect only the prodromal phase of PD.

5. Conclusions

By integrating *in vivo* multi-tracer PET-CT and *ex vivo* immunohistochemical assessments, our results highlight the usefulness of the combined analyses of [^{18}F]-FP-CIT and [^{18}F]-FDG as early biomarkers to detect the manifestations of compromised nigrostriatal dopaminergic signalling, impaired brain metabolism, and disrupted connectivity. Therefore, to conclude, the present study shows, for the first time, in a progressive mouse model of PD pathology, that the connectivity among different brain areas is progressively disrupted as seen in patients with PD (Sala et al., 2017). In addition, the study shows that a correlation exists between *in vivo* [^{18}F]-FP-CIT DAT binding and *ex vivo* DAT and TH immunoreactivity in the striatum, confirming the reliability of the MPTPp mouse model as a model that can reproduce the prodromal PD pathological changes, as was previously shown for non-human primates (Bezard et al., 2013; Meissner et al., 2003). This study highlights the usefulness of multi-tracer PET imaging for the early characterization and longitudinal monitoring of PD. The great importance of these findings for the preclinical evaluation of new drugs that can contrast neurodegeneration in PD is evident and deserves further investigation.

Funding source

The present study was supported by grants from the Italian Ministry of University and Research (PRIN #2017LYTE9M, PI: MM and RMM-SB) and (PRIN#2015R9ASHT, PI: MM). The Italian Ministry of University and Research (MIUR) is gratefully acknowledged for yearly FOE funding to the Euro-BioImaging Multi-Modal Molecular Imaging Italian Node (MMMI). MS gratefully thanks the Zardi-Gori Foundation for the financial support (research grant 2021).

CRediT authorship contribution statement

Margherita Tassan Mazzocco: Visualization, Investigation, Formal analysis, Data curation. **Marcello Serra:** Methodology, Investigation, Formal analysis, Data curation. **Marco Maspero:** Investigation. **Angela Coliva:** Investigation. **Luca Presotto:** Software. **Maria Antonietta Casu:** Investigation. **Micaela Morelli:** Supervision, Funding acquisition, Conceptualization. **Rosa Maria Moresco:** Supervision, Conceptualization. **Sara Belloli:** Supervision, Project administration, Methodology, Funding acquisition. **Annalisa Pinna:** Supervision, Project administration, Methodology, Formal analysis, Data curation, Conceptualization.

Declaration of competing interest

None.

Data availability

Data will be made available on request.

Acknowledgements

We thank Pasquale Simonelli and Giovanni Mennuni for technical assistance in *in vivo* PET imaging.

MS, MM, AP thank the Centre for Research University Services (CeSAR) and the "Centro Servizi di Ateneo per gli Stabulari" (CeSASt), for the technical support.

Appendix A. Supplementary data

Supplementary data to this article can be found online at https://doi.org/10.1016/j.expneurol.2024.114704.

References

Araki, T., Mikami, T., Tanji, H., Matsubara, M., Imai, Y., Mizugaki, M., Itoyama, Y., 2001. Biochemical and immunohistological changes in the brain of 1-methyl-4-phenyl-1,2,3,6-tetrahydropyridine (MPTP)-treated mouse. Eur. J. Pharm. Sci. 12, 231–238. https://doi.org/10.1016/S0928-0987(00)00170-6.

Ascherio, A., Schwarzschild, M.A., 2016. The epidemiology of Parkinson's disease: risk factors and prevention. Lancet Neurol. 15, 1257–1272. https://doi.org/10.1016/S1474-4422(16)30230-7.

Baranyi, M., Porceddu, P.F., Gölöncsér, F., Kulcsár, S., Otrokocsi, L., Kittel, Á., Pinna, A., Frau, L., Huleatt, P.B., Khoo, M.-L., Chai, C.L.L., Dunkel, P., Mátyus, P., Morelli, M., Sperlágh, B., 2016. Novel (hetero)arylalkenyl propargylamine compounds are protective in toxin-induced models of Parkinson's disease. Mol. Neurodegener. 11, 6. https://doi.org/10.1186/s13024-015-0067-y.

Bascuñana, P., Thackeray, J.T., Bankstahl, M., Bengel, F.M., Bankstahl, J.P., 2019. Anesthesia and preconditioning induced changes in mouse brain [18F] FDG uptake and kinetics. Mol. Imaging Biol. 21, 1089–1096. https://doi.org/10.1007/s11307-019-01314-9.

Becker, G., Michel, A., Bahri, M.A., Mairet-Coello, G., Lemaire, C., Deprez, T., Freyssin, A., Jacquin, L., Hustadt, F., De Wolf, C., Caruso, M., Frequin, J.-M., Gillent, E., Bezard, E., Garraux, G., Luxen, A., Citron, M., Downey, P., Plenevaux, A., 2021. Monitoring of a progressive functional dopaminergic deficit in the A53T-AAV synuclein rats by combining 6-[18F]fluoro-L-m-tyrosine imaging and motor performances analysis. Neurobiol. Aging 107, 142–152. https://doi.org/10.1016/j.neurobiolaging.2021.07.012.

Bezard, E., Yue, Z., Kirik, D., Spillantini, M.G., 2013. Animal models of Parkinson's disease: limits and relevance to neuroprotection studies. Mov. Disord. 28, 61–70. https://doi.org/10.1002/mds.25168.

Bidesi, N.S.R., Vang Andersen, I., Windhorst, A.D., Shalgunov, V., Herth, M.M., 2021. The role of neuroimaging in Parkinson's disease. J. Neurochem. 159, 660–689. https://doi.org/10.1111/jnc.15516.

Blandini, F., Armentero, M., 2012. Animal models of Parkinson's disease. FEBS J. 279, 1156–1166. https://doi.org/10.1111/j.1742-4658.2012.08491.x.

Boccalini, C., Bortolin, E., Carli, G., Pilotto, A., Galbiati, A., Padovani, A., Ferini-Strambi, L., Perani, D., 2022. Metabolic connectivity of resting-state networks in alpha synucleinopathies, from prodromal to dementia phase. Front. Neurosci. 16, 930735 https://doi.org/10.3389/fnins.2022.930735.

Bové, J., Perier, C., 2012. Neurotoxin-based models of Parkinson's disease. Neuroscience 211, 51–76. https://doi.org/10.1016/j.neuroscience.2011.10.057.

Brooks, D.J., 2016. Molecular imaging of dopamine transporters. Ageing Res. Rev. 30, 114–121. https://doi.org/10.1016/j.arr.2015.12.009.

Carli, G., Caminiti, S.P., Galbiati, A., Marelli, S., Casoni, F., Padovani, A., Ferini-Strambi, L., Perani, D., 2020. *In-vivo* signatures of neurodegeneration in isolated rapid eye movement sleep behaviour disorder. Eur. J. Neurol. 27, 1285–1295. https://doi.org/10.1111/ene.14215.

Casu, M.A., Pisu, C., Lobina, C., Pani, L., 2004. Immunocytochemical study of the forebrain serotonergic innervation in Sardinian alcohol-preferring rats. Psychopharmacology 172, 341–351. https://doi.org/10.1007/s00213-003-1663-z.

Chaudhuri, K.R., Schapira, A.H., 2009. Non-motor symptoms of Parkinson's disease: dopaminergic pathophysiology and treatment. Lancet Neurol. 8, 464–474. https://doi.org/10.1016/S1474-4422(09)70068-7.

Cheng, H., Ulane, C.M., Burke, R.E., 2010. Clinical progression in Parkinson disease and the neurobiology of axons. Ann. Neurol. 67, 715–725. https://doi.org/10.1002/ana.21995.

Chia, L.-G., Ni, D.-R., Cheng, L.-J., Kuo, J.-S., Cheng, F.-C., Dryhurst, G., 1996. Effects of 1-methyl-4-phenyl-1,2,3,6-tetrahydropyridine and 5,7-dihydroxytryptamine on the locomotor activity and striatal amines in C57BL/6 mice. Neurosci. Lett. 218, 67–71. https://doi.org/10.1016/0304-3940(96)13091-3.

Choi, J.G., Huh, E., Ju, I.G., Kim, N., Yun, J., Oh, M.S., 2018. 1-Methyl-4-phenyl-1,2,3,6 tetrahydropyridine/probenecid impairs intestinal motility and olfaction in the early stages of Parkinson's disease in mice. J. Neurol. Sci. 392, 77–82. https://doi.org/10.1016/j.jns.2018.07.011.

Costa, G., Serra, M., Pintori, N., Casu, M.A., Zanda, M.T., Murtas, D., De Luca, M.A., Simola, N., Fattore, L., 2019. The novel psychoactive substance methoxetamine *induces persistent behavioral abnormalities and neurotoxicity in rats.* Neuropharmacology 144, 219–232. https://doi.org/10.1016/j.neuropharm.2018.10.031.

Eckert, T., Barnes, A., Dhawan, V., Frucht, S., Gordon, M.F., Feigin, A.S., Eidelberg, D., 2005. FDG PET in the differential diagnosis of parkinsonian disorders. NeuroImage 26, 912–921. https://doi.org/10.1016/j.neuroimage.2005.03.012.

Eidelberg, D., Moeller, J.R., Dhawan, V., Spetsieris, P., Takikawa, S., Ishikawa, T., Chaly, T., Robeson, W., Margouleff, D., Przedborski, S., Fahn, S., 1994. The metabolic topography of parkinsonism. J. Cereb. Blood Flow Metab. 14, 783–801. https://doi.org/10.1038/jcbfm.1994.99.

European pharmacopoeia, 8th ed., 2013. Council of Europe: European Directorate for the Quality of Medicines and Healthcare, Strasbourg.

Francardo, V., Schmitz, Y., Sulzer, D., Cenci, M.A., 2017. Neuroprotection and neurorestoration as experimental therapeutics for Parkinson's disease. Exp. Neurol. 298, 137–147. https://doi.org/10.1016/j.expneurol.2017.10.001.

Franklin, K., Paxinos, G., 2008. The Mouse Brain in Stereotaxic Coordinates, Compact - 3rd Edition. Academic Press, pp. 1–256.

Gaspar, P., Berger, B., Gay, M., Hamon, M., Cesselin, F., Vigny, A., Javoy-Agid, F., Agid, Y., 1983. Tyrosine hydroxylase and methionine-enkephalin in the human mesencephalon. J. Neurol. Sci. 58, 247–267. https://doi.org/10.1016/0022-510X(83)90221-6.

Grosch, J., Winkler, J., Kohl, Z., 2016. Early degeneration of both dopaminergic and serotonergic axons – a common mechanism in Parkinson's disease. Front. Cell. Neurosci. 10 https://doi.org/10.3389/fncel.2016.00293.

Hansen, A.K., Knudsen, K., Lillethorup, T.P., Landau, A.M., Parbo, P., Fedorova, T., Audrain, H., Bender, D., Østergaard, K., Brooks, D.J., Borghammer, P., 2016. *In vivo* imaging of neuromelanin in Parkinson's disease using ^{18}F-AV-1451 PET. Brain 139, 2039–2049. https://doi.org/10.1093/brain/aww098.

Holtbernd, F., Gagnon, J.-F., Postuma, R.B., Ma, Y., Tang, C.C., Feigin, A., Dhawan, V., Vendette, M., Soucy, J.-P., Eidelberg, D., Montplaisir, J., 2014. Abnormal metabolic network activity in REM sleep behavior disorder. Neurology 82, 620–627. https://doi.org/10.1212/WNL.0000000000000130.

Horwitz, B., Duara, R., Rapoport, S.I., 1984. Intercorrelations of glucose metabolic rates between brain regions: application to healthy males in a state of reduced sensory input. J. Cereb. Blood Flow Metab. 4, 484–499. https://doi.org/10.1038/jcbfm.1984.73.

Im, H.-J., Hwang, D.W., Lee, H.K., Jang, J., Lee, S., Youn, H., Jin, Y., Kim, S.U., Kim, E.E., Kim, Y.S., Lee, D.S., 2013. In vivo visualization and monitoring of viable neural stem cells using noninvasive bioluminescence imaging in the 6-hydroxydopamine-induced mouse model of Parkinson disease. Mol. Imaging 12, 224–234.

Im, H.-J., Hahm, J., Kang, H., Choi, H., Lee, H., Hwang, D.W., Kim, E.E., Chung, J.-K., Lee, D.S., 2016. Disrupted brain metabolic connectivity in a 6-OHDA-induced mouse model of Parkinson's disease examined using persistent homology-based analysis. Sci. Rep. 6, 33875. https://doi.org/10.1038/srep33875.

Iranzo, A., Tolosa, E., Gelpi, E., Molinuevo, J.L., Valldeoriola, F., Serradell, M., Sanchez-Valle, R., Vilaseca, I., Lomeña, F., Vilas, D., Lladó, A., Gaig, C., Santamaria, J., 2013. Neurodegenerative disease status and post-mortem pathology in idiopathic rapid-eye-movement sleep behaviour disorder: an observational cohort study. Lancet Neurol. 12, 443–453. https://doi.org/10.1016/S1474-4422(13)70056-5.

Ishibashi, K., Oda, K., Ishiwata, K., Ishii, K., 2014. Comparison of dopamine transporter decline in a patient with Parkinson's disease and normal aging effect. J. Neurol. Sci. 339, 207–209. https://doi.org/10.1016/j.jns.2014.01.015.

Jankovic, J., 2008. Parkinson's disease: clinical features and diagnosis. J. Neurol. Neurosurg. Psychiatry 79, 368–376. https://doi.org/10.1136/jnnp.2007.131045.

Kerstens, V.S., Fazio, P., Sundgren, M., Halldin, C., Svenningsson, P., Varrone, A., 2023. [18F]FE-PE2I DAT correlates with Parkinson's disease duration, stage, and rigidity/bradykinesia scores: a PET radioligand validation study. EJNMMI Res. 13, 29. https://doi.org/10.1186/s13550-023-00974-7.

Kordower, J.H., Olanow, C.W., Dodiya, H.B., Chu, Y., Beach, T.G., Adler, C.H., Halliday, G.M., Bartus, R.T., 2013. Disease duration and the integrity of the nigrostriatal system in Parkinson's disease. Brain 136, 2419–2431. https://doi.org/10.1093/brain/awt192.

Lee, S.J., Oh, S.J., Chi, D.Y., Kang, S.H., Kil, H.S., Kim, J.S., Moon, D.H., 2007. One-step high-radiochemical-yield synthesis of [18F]FP-CIT using a protic solvent system. Nucl. Med. Biol. 34, 345–351. https://doi.org/10.1016/j.nucmedbio.2007.02.007.

Li, X., Zhang, Q., Qin, Y., Li, Y., Mutaerbieke, N., Zhao, X., Yibulayin, A., 2020. Positron emission tomography/computed tomography dual imaging using 18-fluorine flurodeoxyglucose and 11C-labeled 2-β-carbomethoxy-3-β-(4-fluorophenyl) tropane for the severity assessment of Parkinson disease. Medicine 99, e19662. https://doi.org/10.1097/MD.0000000000019662.

Luchtman, D.W., Shao, D., Song, C., 2009. Behavior, neurotransmitters and inflammation in three regimens of the MPTP mouse model of Parkinson's disease. Physiol. Behav. 98, 130–138. https://doi.org/10.1016/j.physbeh.2009.04.021.

Luchtman, D.W., Meng, Q., Song, C., 2012. Ethyl-eicosapentaenoate (E-EPA) attenuates *motor impairments and inflammation in the MPTP-probenecid mouse model of* Parkinson's disease. Behav. Brain Res. 226, 386–396. https://doi.org/10.1016/j.bbr.2011.09.033.

Matthews, D.C., Lerman, H., Lukic, A., Andrews, R.D., Mirelman, A., Wernick, M.N., Giladi, N., Strother, S.C., Evans, K.C., Cedarbaum, J.M., Even-Sapir, E., 2018. FDG PET Parkinson's disease-related pattern as a biomarker for clinical trials in early stage disease. NeuroImage Clin. 20, 572–579. https://doi.org/10.1016/j.nicl.2018.08.006.

Matuskey, D., Tinaz, S., Wilcox, K.C., Naganawa, M., Toyonaga, T., Dias, M., Henry, S., Pittman, B., Ropchan, J., Nabulsi, N., Suridjan, I., Comley, R.A., Huang, Y.,

Finnema, S.J., Carson, R.E., 2020. Synaptic changes in Parkinson disease assessed with in vivo imaging. Ann. Neurol. 87, 329–338. https://doi.org/10.1002/ana.25682.

Meissner, W., Prunier, C., Guilloteau, D., Chalon, S., Gross, C.E., Bezard, E., 2003. Time-course of nigrostriatal degeneration in a progressive MPTP-lesioned macaque model of Parkinson's disease. MN 28, 209–218. https://doi.org/10.1385/MN:28:3:209.

Meles, S.K., Oertel, W.H., Leenders, K.L., 2021. Circuit imaging biomarkers in preclinical and prodromal Parkinson's disease. Mol. Med. 27, 111. https://doi.org/10.1186/s10020-021-00327-x.

Meredith, G.E., Kang, U.J., 2006. Behavioral models of Parkinson's disease in rodents: a new look at an old problem. Mov. Disord. 21, 1595–1606. https://doi.org/10.1002/mds.21010.

Meredith, G.E., Rademacher, D.J., 2011. MPTP mouse models of Parkinson's disease: an update. J. Parkinsons Dis. 1, 19–33. https://doi.org/10.3233/JPD-2011-11023.

Mitchell, T., Lehéricy, S., Chiu, S.Y., Strafella, A.P., Stoessl, A.J., Vaillancourt, D.E., 2021. Emerging neuroimaging biomarkers across disease stage in Parkinson disease: a review. JAMA Neurol. 78, 1262. https://doi.org/10.1001/jamaneurol.2021.1312.

Nandhagopal, R., Kuramoto, L., Schulzer, M., Mak, E., Cragg, J., Lee, C.S., McKenzie, J., McCormick, S., Samii, A., Troiano, A., Ruth, T.J., Sossi, V., De La Fuente-Fernandez, R., Calne, D.B., Stoessl, A.J., 2009. Longitudinal progression of sporadic Parkinson's disease: a multi-tracer positron emission tomography study. Brain 132, 2970–2979. https://doi.org/10.1093/brain/awp209.

Noyce, A.J., Dickson, J., Rees, R.N., Bestwick, J.P., Isaias, I.U., Politis, M., Giovannoni, G., Warner, T.T., Lees, A.J., Schrag, A., 2018. Dopamine reuptake transporter–single-photon emission computed tomography and transcranial sonography as imaging markers of prediagnostic Parkinson's disease. Mov. Disord. 33, 478–482. https://doi.org/10.1002/mds.27282.

Obeso, J.A., Stamelou, M., Goetz, C.G., Poewe, W., Lang, A.E., Weintraub, D., Burn, D., Halliday, G.M., Bezard, E., Przedborski, S., Lehericy, S., Brooks, D.J., Rothwell, J.C., Hallett, M., DeLong, M.R., Marras, C., Tanner, C.M., Ross, G.W., Langston, J.W., Klein, C., Bonifati, V., Jankovic, J., Lozano, A.M., Deuschl, G., Bergman, H., Tolosa, E., Rodriguez-Violante, M., Fahn, S., Postuma, R.B., Berg, D., Marek, K., Standaert, D.G., Surmeier, D.J., Olanow, C.W., Kordower, J.H., Calabresi, P., Schapira, A.H.V., Stoessl, A.J., 2017. Past, present, and future of Parkinson's disease: a special essay on the 200th Anniversary of the Shaking Palsy. Mov. Disord. 32, 1264–1310. https://doi.org/10.1002/mds.27115.

Parekh, P., Serra, M., Allaw, M., Perra, M., Marongiu, J., Tolle, G., Pinna, A., Casu, M.A., Manconi, M., Caboni, P., Manzoni, O.J.J., Morelli, M., 2022. Characterization of Nasco grape pomace-loaded nutriosomes and their neuroprotective effects in the MPTP mouse model of Parkinson's disease. Front. Pharmacol. 13, 935784 https://doi.org/10.3389/fphar.2022.935784.

Peng, S., Eidelberg, D., Ma, Y., 2014. Brain network markers of abnormal cerebral glucose metabolism and blood flow in Parkinson's disease. Neurosci. Bull. 30, 823–837. https://doi.org/10.1007/s12264-014-1472-x.

Perez, X.A., Parameswaran, N., Huang, L.Z., O'Leary, K.T., Quik, M., 2008. Pre-synaptic dopaminergic compensation after moderate nigrostriatal damage in non-human primates. J. Neurochem. 105, 1861–1872. https://doi.org/10.1111/j.1471-4159.2008.05268.x.

Perlmutter, J.S., Norris, S.A., 2014. Neuroimaging biomarkers for P arkinson disease: facts and fantasy. Ann. Neurol. 76, 769–783. https://doi.org/10.1002/ana.24291.

Perovnik, M., Rus, T., Schindlbeck, K.A., Eidelberg, D., 2023. Functional brain networks in the evaluation of patients with neurodegenerative disorders. Nat. Rev. Neurol. 19, 73–90. https://doi.org/10.1038/s41582-022-00753-3.

Petroske, E., Meredith, G.E., Callen, S., Totterdell, S., Lau, Y.-S., 2001. Mouse model of Parkinsonism: a comparison between subacute MPTP and chronic MPTP/probenecid treatment. Neuroscience 106, 589–601. https://doi.org/10.1016/S0306-4522(01)00295-0.

Pinna, A., Napolitano, F., Pelosi, B., Di Maio, A., Wardas, J., Casu, M.A., Costa, G., Migliarini, S., Calabresi, P., Pasqualetti, M., Morelli, M., Usiello, A., 2016. The S mall *GTP - B inding P rotein R hes I nfluences N igrostriatal- D ependent M otor B ehavior* D uring A ging. Mov. Disord. 31, 583–589. https://doi.org/10.1002/mds.26489.

Pisanu, A., Lecca, D., Valentini, V., Bahi, A., Dreyer, J.-L., Cacciapaglia, F., Scifo, A., Piras, G., Cadoni, C., Di Chiara, G., 2015. Impairment of acquisition of intravenous cocaine self-administration by RNA-interference of dopamine D1-receptors in the nucleus accumbens shell. Neuropharmacology 89, 398–411. https://doi.org/10.1016/j.neuropharm.2014.10.018.

Postuma, R.B., Iranzo, A., Hu, M., Högl, B., Boeve, B.F., Manni, R., Oertel, W.H., Arnulf, I., Ferini-Strambi, L., Puligheddu, M., Antelmi, E., Cochen De Cock, V., Arnaldi, D., Mollenhauer, B., Videnovic, A., Sonka, K., Jung, K.-Y., Kunz, D., Dauvilliers, Y., Provini, F., Lewis, S.J., Buskova, J., Pavlova, M., Heidbreder, A., Montplaisir, J.Y., Santamaria, J., Barber, T.R., Stefani, A., St Louis, E.K., Terzaghi, M., Janzen, A., Leu-Semenescu, S., Plazzi, G., Nobili, F., Sixel-Doering, F., Dusek, P., Bes, F., Cortelli, P., Ehgoetz Martens, K., Gagnon, J.-F., Gaig, C., Zucconi, M., Trenkwalder, C., Gan-Or, Z., Lo, C., Rolinski, M., Mahlknecht, P., Holzknecht, E., Boeve, A.R., Teigen, L.N., Toscano, G., Mayer, G., Morbelli, S., Dawson, B., Pelletier, A., 2019. Risk and predictors of dementia and parkinsonism in idiopathic REM sleep behaviour disorder: a multicentre study. Brain 142, 744–759. https://doi.org/10.1093/brain/awz030.

Presotto, L., Bettinardi, V., Mercatelli, D., Picchio, M., Morari, M., Moresco, R.M., Belloli, S., 2022. Development of a new toolbox for mouse PET–CT brain image analysis fully based on CT images and validation in a PD mouse model. Sci. Rep. 12, 15822. https://doi.org/10.1038/s41598-022-19872-4.

Sala, A., Caminiti, S.P., Presotto, L., Premi, E., Pilotto, A., Turrone, R., Cosseddu, M., Alberici, A., Paghera, B., Borroni, B., Padovani, A., Perani, D., 2017. Altered brain metabolic connectivity at multiscale level in early Parkinson's disease. Sci. Rep. 7, 4256. https://doi.org/10.1038/s41598-017-04102-z.

Schenck, C.H., Boeve, B.F., Mahowald, M.W., 2013. Delayed emergence of a parkinsonian disorder or dementia in 81% of older men initially diagnosed with idiopathic rapid eye movement sleep behavior disorder: a 16-year update on a previously reported series. Sleep Med. 14, 744–748. https://doi.org/10.1016/j.sleep.2012.10.009.

Schindlbeck, K.A., Vo, A., Nguyen, N., Tang, C.C., Niethammer, M., Dhawan, V., Brandt, V., Saunders-Pullman, R., Bressman, S.B., Eidelberg, D., 2020. LRRK2 and GBA variants exert distinct influences on Parkinson's disease-specific metabolic networks. Cereb. Cortex 30, 2867–2878. https://doi.org/10.1093/cercor/bhz280.

Schintu, N., Frau, L., Ibba, M., Garau, A., Carboni, E., Carta, A.R., 2009. Progressive dopaminergic degeneration in the chronic MPTPp mouse model of Parkinson's disease. Neurotox. Res. 16, 127–139. https://doi.org/10.1007/s12640-009-9061-x.

Schumm, S., Sebban, C., Cohen-Salmon, C., Callebert, J., Launay, J., Golmard, J., Boussicault, L., Petropoulos, I., Hild, A., Rousselet, E., Prigent, A., Friguet, B., Mariani, J., Hirsch, E.C., 2012. Aging of the dopaminergic system and motor behavior in mice intoxicated with the parkinsonian toxin 1-methyl-4-phenyl-1,2,3,6-tetrahydropyridine. J. Neurochem. 122, 1032–1046. https://doi.org/10.1111/j.1471-4159.2012.07837.x.

Serra, M., Di Maio, A., Bassareo, V., Nuzzo, T., Errico, F., Servillo, F., Capasso, M., Parekh, P., Li, Q., Thiolat, M.-L., Bezard, E., Calabresi, P., Sulzer, D., Carta, M., Morelli, M., Usiello, A., 2023. Perturbation of serine enantiomers homeostasis in the striatum of MPTP-lesioned monkeys and mice reflects the extent of dopaminergic midbrain degeneration. Neurobiol. Dis. 184, 106226 https://doi.org/10.1016/j.nbd.2023.106226.

Shimoji, K., Ravasi, L., Schmidt, K., Soto-Montenegro, M.L., Esaki, T., Seidel, J., Jagoda, E., Sokoloff, L., Green, M.V., Eckelman, W.C., 2004. Measurement of cerebral glucose metabolic rates in the anesthetized rat by dynamic scanning with 18F-FDG, the ATLAS small animal PET scanner, and arterial blood sampling. J. Nucl. Med. 45, 665–672.

Simuni, T., Siderowf, A., Lasch, S., Coffey, C.S., Caspell-Garcia, C., Jennings, D., Tanner, C.M., Trojanowski, J.Q., Shaw, L.M., Seibyl, J., Schuff, N., Singleton, A., Kieburtz, K., Toga, A.W., Mollenhauer, B., Galasko, D., Chahine, L.M., Weintraub, D., Foroud, T., Tosun, D., Poston, K., Arnedo, V., Frasier, M., Sherer, T., Chowdhury, S., Marek, K., the Parkinson's Progression Marker Initiative*, 2018. Longitudinal change of clinical and biological measures in early Parkinson's disease: Parkinson's progression markers initiative cohort. Mov. Disord. 33, 771–782. https://doi.org/10.1002/mds.27361.

Spetsieris, P.G., Eidelberg, D., 2021. Spectral guided sparse inverse covariance estimation of metabolic networks in Parkinson's disease. NeuroImage 226, 117568. https://doi.org/10.1016/j.neuroimage.2020.117568.

Spetsieris, P.G., Eidelberg, D., 2023. Parkinson's disease progression: increasing expression of an invariant common core subnetwork. NeuroImage Clin. 39, 103488 https://doi.org/10.1016/j.nicl.2023.103488.

Stoessl, A.J., 2007. Positron emission tomography in premotor Parkinson's disease. Parkinsonism Relat. Disord. 13, S421–S424. https://doi.org/10.1016/S1353-8020(08)70041-5.

Taguchi, T., Ikuno, M., Yamakado, H., Takahashi, R., 2020. Animal model for prodromal *Parkinson's disease. IJMS 21, 1961. https://doi.org/10.3390/ijms21061961.*

Tanji, H., Araki, T., Nagasawa, H., Itoyama, Y., 1999. Differential vulnerability of dopamine receptors in the mouse brain treated with MPTP. Brain Res. 824, 224–231. https://doi.org/10.1016/S0006-8993(99)01209-3.

Tassan Mazzocco, M., Murtaj, V., Martins, D., Schellino, R., Coliva, A., Toninelli, E., Vercelli, A., Turkheimer, F., Belloli, S., Moresco, R.M., 2023. Exploring the neuroprotective effects of montelukast on brain inflammation and metabolism in a rat model of quinolinic acid-induced striatal neurotoxicity. J. Neuroinflammation 20, 34. https://doi.org/10.1186/s12974-023-02714-z.

Tolosa, E., Garrido, A., Scholz, S.W., Poewe, W., 2021. Challenges in the diagnosis of Parkinson's disease. Lancet Neurol. 20, 385–397. https://doi.org/10.1016/S1474-4422(21)00030-2.

Wang, J., Jiang, H., Xie, J.-X., 2004. Time dependent effects of 6-OHDA lesions on Iron level and neuronal loss in rat nigrostriatal system. Neurochem. Res. 29, 2239–2243. https://doi.org/10.1007/s11064-004-7031-5.